THE JOURNAL OF BIOLOGICAL CHEMISTRY VOL. 286, NO. 45, pp. 39328–39335, November 11, 2011

Waixenicin A Inhibits Cell Proliferation through Magnesium-dependent Block of Transient Receptor Potential Melastatin 7 (TRPM7) Channels*[S]

Received for publication, May 24, 2011, and in revised form, September 8, 2011 Published, JBC Papers in Press, September 16, 2011, DOI 10.1074/jbc.M111.264341

Susanna Zierler[‡1], Guangmin Yao[§2], Zheng Zhang[‡], W. Cedric Kuo[§], Peter Pörzgen[§], Reinhold Penner[‡], F. David Horgen[§], and Andrea Fleig[‡3]

From the [‡]Center for Biomedical Research, The Queen's Medical Center and John A. Burns School of Medicine, University of Hawaii, Honolulu, Hawaii 96813 and the [§]Laboratory of Marine Biological Chemistry, Department of Natural Sciences, Hawaii Pacific University, Kaneohe, Hawaii 96744

Background: TRPM7 channels are key regulators of cell growth and proliferation.
Results: A natural compound from a Hawaiian soft coral blocks TRPM7 currents and inhibits proliferation.
Conclusion: Waixenicin A represents the first potent and relatively specific inhibitor of TRPM7 ion channels.
Significance: Waixenicin A or structural analogs may have cancer-specific therapeutic potential.

Transient receptor potential melastatin 7 (TRPM7) channels represent the major magnesium-uptake mechanism in mammalian cells and are key regulators of cell growth and proliferation. They are expressed abundantly in a variety of human carcinoma cells controlling survival, growth, and migration. These characteristics are the basis for recent interest in the channel as a target for cancer therapeutics. We screened a chemical library of marine organism-derived extracts and identified waixenicin A from the soft coral *Sarcothelia edmondsoni* as a strong inhibitor of overexpressed and native TRPM7. Waixenicin A activity was cytosolic and potentiated by intracellular free magnesium (Mg^{2+}) concentration. Mutating a Mg^{2+} binding site on the TRPM7 kinase domain reduced the potency of the compound, whereas kinase deletion enhanced its efficacy independent of Mg^{2+}. Waixenicin A failed to inhibit the closely homologous TRPM6 channel and did not significantly affect TRPM2, TRPM4, and Ca^{2+} release-activated Ca^{2+} current channels. Therefore, waixenicin A represents the first potent and relatively specific inhibitor of TRPM7 ion channels. Consistent with TRPM7 inhibition, the compound blocked cell proliferation in human Jurkat T-cells and rat basophilic leukemia cells. Based on the ability of the compound to inhibit cell proliferation through Mg^{2+}-dependent block of TRPM7, waixenicin A, or structural analogs may have cancer-specific therapeutic potential, particularly because certain cancers accumulate cytosolic Mg^{2+}.

TRPM6 and TRPM7 are members of the melastatin-like transient receptor potential (TRPM)[4] subfamily. They possess an ion channel and a functional α-kinase domain and have been implicated in Mg^{2+} homeostasis (1–3). Originally, TRPM6 was thought to regulate systemic (4, 5) and TRPM7 cellular Mg^{2+} homeostasis (6). However, recent findings demonstrate that TRPM7 also is critically involved in systemic Mg^{2+} regulation of mammalian organisms, with the channel function facilitating cellular Mg^{2+} influx and the kinase activity regulating Mg^{2+} absorption (6). Both activities are interdependent in that Mg^{2+} enters through the channel pore and the kinase domain requires Mg^{2+} ions to function, whereas both Mg^{2+} and Mg-ATP provide a negative feedback loop by regulating channel activity through binding at specific sites on the kinase domain (2, 7, 8).

Suppression of divalent ion conductance via TRPM7 (9) protects neurons from reperfusion injury after cerebral ischemia (10, 11). When silencing TRPM7, Ca^{2+} influx and neuronal cell death following ischemic injury are blocked, and neuronal recovery is enhanced (12), linking TRPM7 to neurodegenerative diseases (10, 12–15). TRPM7 has also been implicated as a regulator of cell proliferation (16–20), inducing cell cycle arrest if blocked. This is based on channel function in Mg^{2+} transport because cell growth can be restored by Mg^{2+} supplementation (2, 8, 18, 21, 22). Mg^{2+} is involved in essentially every step of cell proliferation, with cancerous cell growth representing the most detrimental effect of deregulated proliferation. Interestingly, cancerous tissue acts as a Mg^{2+} trap by accumulating Mg^{2+} at the expense of plasma or surrounding tissues (23, 24). *In vivo* experiments revealed a 60% reduction in primary tumor growth and angiogenesis in Mg^{2+}-deficient mice compared with Mg^{2+}-sufficient controls. When reintroducing Mg^{2+} into the diet of hypomagnesemic mice, tumors rapidly regained proliferation capacity and became 40% larger than those grown in

* This work was supported, in whole or in part, by National Institutes of Health Grants P01GM078195 (to A. F.), P20 RR-016467 (to F. D. H.), and 5G12 RR003061-22 (University of Hawaii Imaging Core). This work was also supported by an American Society of Pharmacognosy Undergraduate Research Award (to W. C. K.) and Austrian Science Fund Grant J2784 (to S. Z.).
[S] The on-line version of this article (available at http://www.jbc.org) contains supplemental "Experimental Procedures" and Figs. S1–S6.
[1] Present address: Walther-Straub-Institute for Pharmacology and Toxicology, Ludwig-Maximilians-University Munich, 80336 Munich, Germany.
[2] Present address: School of Pharmacy, Tongji Medical College, Huazhong University of Science and Technology, Wuhan 430030, China.
[3] To whom correspondence should be addressed: 1301 Punchbowl St., Honolulu, HI 96813. E-mail: afleig@hawaii.edu.

[4] The abbreviations used are: TRPM, transient receptor potential melastatin; CRAC, Ca^{2+}-release activated Ca^{2+} current; RBL, rat basophilic leukemia; pA, picoAmpere; pF, picoFarad.

Mg^{2+}-sufficient mice (24). It is tempting to speculate that TRPM7 is involved in these processes.

TRPM7 is expressed abundantly in a variety of human carcinoma cells including gastric adenocarcinoma, breast cancer, and human head and neck carcinoma cells. Suppression of TRPM7 by siRNA and/or non-selective inhibitors has been shown to inhibit the growth of these cell types (18, 19, 21). Overexpression of TRPM7 was detected in breast cancer tissues, and TRPM7 expression levels correlate with their proliferative potential (18). Moreover, TRPM7 has been shown to regulate migration of human nasopharyngeal carcinoma cells (25), indicating a potential role in metastasis.

Currently, there is no known specific inhibitor for TRPM7. Although several compounds have been reported to affect TRPM7, including 2-aminoethyl-diphenylborinate (1), lanthanum (La^{3+}), gadolinium (Gd^{3+}), SKF-96365 (9, 26–28), spermine (27), carvacrol (29), and 5-lipoxygenase inhibitors (30), they lack either potency or specificity or both and are therefore of limited use. Concentrations between 50 and 500 μM of the cell-permeant compound 2-aminoethyl-diphenylborinate have been shown to reduce TRPM7 currents, while enhancing TRPM6 currents, providing an experimental tool to distinguish between both channel types (1). However, 2-aminoethyl-diphenylborinate can also affect Ca^{2+} release-activated Ca^{2+} current (CRAC) channels as well as a number of other ion channels in a dose-dependent manner (31–33), thus disqualifying it as specific inhibitor for TRPM7. La^{3+}, Gd^{3+}, and SKF-96365 block TRPM7 but also inhibit other Ca^{2+}-permeable channels, including CRAC channels (9, 26–28). The polyamine spermine has been shown to distinguish between CRAC and TRPM7 channels, blocking only monovalent TRPM7 currents at micromolar concentrations (27). However, spermine and polyamines also inhibit K^+ and other cation channels (34–37). Recently, carvacrol was shown to inhibit TRPM7 but also lacks specificity as it inhibits several TRPC and TRPM channels (29) and activates TRPV3 and TRPA1 channels. The 5-lipoxygenase inhibitors, nordihydroguaiaretic acid, AA861, and MK886, have also been shown to affect TRPM7 channels in the micromolar range and independently of lipoxygenase activity (30), but they also affect K^+ and Cl^- channels (38–41). A pharmacological modulator for the TRPM7 ion channel could be beneficial not only as an experimental tool but also therapeutically in cardiac, neuropathological, or anti-cancer treatment. We therefore screened an in-house library of marine-derived natural products and identified waixenicin A as a highly potent and relatively selective inhibitor for TRPM7 that effectively suppressed cell growth and proliferation.

EXPERIMENTAL PROCEDURES

For detailed methods, see the supplemental "Experimental Procedures."

Animal Material and Cell Line Origin—Freeze-dried samples of *Sarcothelia edmondsoni* (formerly known as *Anthelia edmondsoni*) were extracted in methanol and reconstituted in methanol/ethyl acetate/*t*-butyl methyl ether (60:30:10) (MET) and diluted in Krebs-Ringer-HEPES buffer (135 mM NaCl, 5 mM KCl, 1.5 mM $MgCl_2$, 1.5 mM $CaCl_2$, 20 mM HEPES, and 5.6 mM glucose). HEK293 cell lines were obtained from Dr. Andrew Scharenberg's laboratory (TRPM2, TRPM7-wt, and mutants) and Dr. Jean-Pierre Kinet's laboratory (TRPM4). rat basophilic leukemia cells (RBL1) cells were acquired through ATCC. Human Jurkat T-lymphocytes were obtained from Dr. Kinet's laboratory. No authentication was performed by the authors other than testing for ion channel expression through electrophysiological measurements.

Isolation of Waixenicin A—Fractionation of the soft coral extract was guided by LC-MS data (electrospray ionization; ion trap analyzer; Thermo Finnigan LCQ Deca XP) obtained for the extract peak corresponding to the highest TRPM7 activity. The extract was subjected to vacuum liquid chromatography and fraction eluting with dichloromethane/methanol (95:5) concentrated the targeted compound. Repeated semi-preparative reversed phase HPLC led to the isolation of waixenicin A (see Fig. 1*E*), which was identified by comparison of NMR data and optical rotation with literature values (42). Purity of our waixenicin A sample was determined to be >95%, and lyophilized waixenicin A was dissolved in 60 μl of methanol (100 μM stock solution) stored at −20 °C.

Statistical Analysis—Data represent the mean of individual experiments ± S.E. and Student's *t* test assessed $p < 0.05$ as statistically significant.

RESULTS

Waixenicin A Is TRPM7 Inhibitor Isolated from Hawaiian Soft Coral Sarcothelia edmondsoni—We screened an in-house chemical library of 1100 marine organism-derived extracts in a high-throughput assay system that measures the fluorescence quench of intracellular fura-2 by Mn^{2+} ions in HEK293 cells overexpressing murine TRPM7 (43). We identified the organic extract of the soft coral *S. edmondsoni* (synonym: *Anthelia edmondsoni*) as a strong inhibitor of TRPM7-mediated Mn^{2+} influx at a concentration of 30 μg/ml (Fig. 1*A*). The assay was further employed to identify the major active component by bioassay-linked fractionation (44). Fig. 1*B* shows the HPLC chromatogram and bioassay profile for the resulting 70 fractions. The highest activity concentrated in fractions eluting at 16.5–18 min, corresponding to the UV peak at 17.1 min. The active peak was characterized by HPLC coupled to a mass spectrometer (LC-MS), leading to the isolation and identification of waixenicin A (Fig. 1*E*), a known metabolite from *S. edmondsoni* (42). Waixenicin A inhibited TRPM7-mediated Mn^{2+} quench in a dose-dependent manner (Fig. 1*C*) and demonstrated an IC_{50} of the maximal slope of the Mn^{2+} quench of 12 μM (Fig. 1*D*).

Analysis of waixenicin A in patch clamp experiments (Fig. 2) confirmed the inhibitory effect on TRPM7. To activate TRPM7 currents, intracellular Mg^{2+} and Mg-ATP were washed out by perfusion with Mg^{2+}- and ATP-free internal solution. Whole-cell currents were elicited by voltage ramps from −100 to +100 mV delivered at 0.5 Hz, and current amplitudes were extracted at +80 mV and plotted *versus* time. TRPM7 currents reached a plateau of ~130 pico-Ampere per pico-Farad within 200 s, whereas application of 10 μM waixenicin A for 300 s inhibited TRPM7 by ~50% (Fig. 2, *A* and *B*). The dose-response analysis of waixenicin A-mediated inhibition of TRPM7 revealed an IC_{50} of 7 μM (Fig. 2*E*). Outward

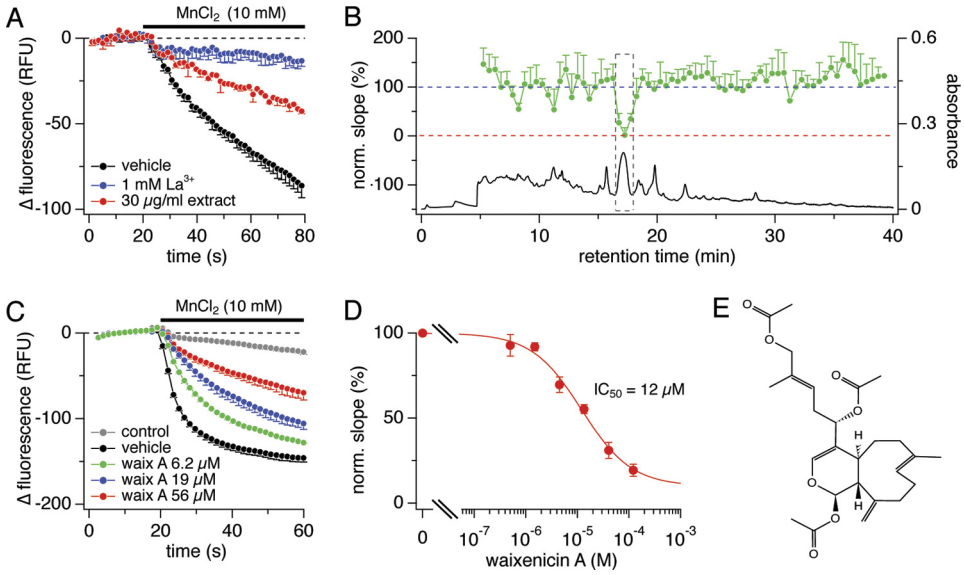

FIGURE 1. **Screening assay identifies waixenicin A as TRPM7 inhibitor**. *A*, decrease in relative fluorescence units (*RFU*) following 10 mM $MnCl_2$ application in HEK293-TRPM7. Vehicle was negative control (*black*, $n = 10$). La^{3+} (*blue*, $n = 10$) and the extract (*red*, $n = 2$) reduced Mn^{2+}-induced fluorescence quench. *Error bars* represent S.D. *B*, HPLC chromatogram (UV absorbance at 220–240 nm) of extract fractionation (*black*) and bioassay profile for the fractions (*green*) plotted as normalized slopes of fluorescence quench against retention time. *Error bars* represent S.D. *C*, HEK293-TRPM7 cells were incubated with waixenicin A for 15 min before 10 mM $MnCl_2$ application: uninduced HEK293 control (*gray*, $n = 8$), vehicle (*black*, $n = 8$), waixenicin A at 6.2 μM (*green*, $n = 3$), 19 μM (*blue*, $n = 3$), and 56 μM (*red*, $n = 3$). *D*, maximum slopes of fluorescence quench normalized to vehicle control, plotted against concentration, and approximated by dose-response fit ($n = 3–8$). *Error bars* represent S.D. *E*, chemical structure of waixenicin A (relative configuration shown).

and inward currents were affected similarly (supplemental Fig. S1*A*). In the presence of physiological 700 μM free internal Mg^{2+} ($[Mg^{2+}]_i$), TRPM7 currents were smaller, leveling off at ~30 pA/pF (Fig. 2, *C* and *D*), and 10 μM waixenicin A completely blocked the current. The dose-response curve obtained with 700 μM $[Mg^{2+}]_i$ dramatically shifted the IC_{50} from 7 μM in 0 $[Mg^{2+}]_i$ to 16 nM (Fig. 2*F*). Inward and outward currents were blocked similarly (supplemental Fig. S1*B*).

Additional removal of extracellular Mg^{2+} resulted in a 2-fold increase of TRPM7 currents compared with 2 mM extracellular Mg^{2+} (supplemental Fig. S2*A*), indicating that Mg^{2+} influx through TRPM7 contributes to reduced channel activity. 10 μM waixenicin A was less effective in suppressing TRPM7 in extracellular Mg^{2+}-free conditions, causing 30% inhibition compared with 50% when extracellular Mg^{2+} was present. This suggests that waixenicin A synergizes with intracellular Mg^{2+} in suppressing channel activity.

Blocking Potency of Waixenicin A Is Regulated by Intracellular Mg^{2+}—We investigated the Mg^{2+} dependence of waixenicin A by applying 10 μM waixenicin A at various internal Mg^{2+} concentrations. We observed an IC_{50} of 80 μM $[Mg^{2+}]_i$ for both outward (Fig. 3*A*) and inward TRPM7 currents (supplemental Fig. S1*C*). Thus, 10 μM waixenicin A exhibited an equivalent blocking potency as millimolar levels of Mg-ATP as the IC_{50} values for $[Mg^{2+}]_i$ in the presence of 2–6 mM Mg-ATP are 110–250 μM (7). This would suggest that Mg^{2+} facilitates waixenicin A binding to TRPM7 or that the compound increases efficacy of block by free internal Mg^{2+}.

The Lys-1648 residue within the TRPM7 kinase domain represents one of the inhibitory sites for Mg^{2+} and Mg-ATP (2, 7, 8). A stable cell line inducibly overexpressing the K1648R mutant has a reduced Mg^{2+} sensitivity with an IC_{50} for Mg^{2+} of ~3 mM compared with ~700 μM for TRPM7-wt (8). We first assessed the dose-response behavior of waixenicin A, whereas $[Mg^{2+}]_i$ was clamped to 700 μM. The dose-response relationships in Fig. 3*B* reflect normalized current amplitudes at +80 mV extracted after 300 s of waixenicin A exposure. They demonstrate that the K1648R mutant has a 150-fold reduced sensitivity to the Mg^{2+}-dependent inhibition of waixenicin A compared with TRPM7-wt (IC_{50} = 2.5 μM *versus* 16 nM, respectively). We next assessed the efficacy of 10 μM waixenicin A to inhibit TRPM7-K1648R currents while varying $[Mg^{2+}]_i$. 10 μM waixenicin A (Fig. 3*A*) shifted waixenicin A sensitivity to Mg^{2+}-dependent inhibition of the K1648R mutant by almost 3-fold compared with TRPM7-wt (IC_{50} = 200 μM *versus* 80 μM, respectively). Together, these results suggest that the Mg^{2+} binding site on the kinase domain contributes to the inhibitory potency of waixenicin A.

We next tested compound activity in HEK293 cells overexpressing a TRPM7 protein lacking the entire kinase domain (TRPM7-ΔK). Despite the lack of the kinase domain and its Mg^{2+} binding site, the ΔK mutant has been shown to be even more sensitive to intracellular Mg^{2+} levels, as kinase truncation appears to expose a second high affinity Mg^{2+} binding site on the channel (8). Thus, we used Mg^{2+}-free intracellular solutions to elicit TRPM7-ΔK currents (Fig. 3, *C* and *D*). Waixenicin A (10 μM) was still able to inhibit TRPM7 conductance completely and the block was even more pronounced than in TRPM7-wt (*cf.* Fig. 2*A* and supplemental Fig. S2*A*). In the complete absence of both intra- and extracellular Mg^{2+}, TRPM7-ΔK currents were larger but were still completely suppressed by 10 μM waixenicin A (supplemental Fig. S2*B*). Even 300 nM waixenicin A completely inhibited TRPM7-ΔK, suggesting a direct and Mg^{2+}-independent high affinity mode of action.

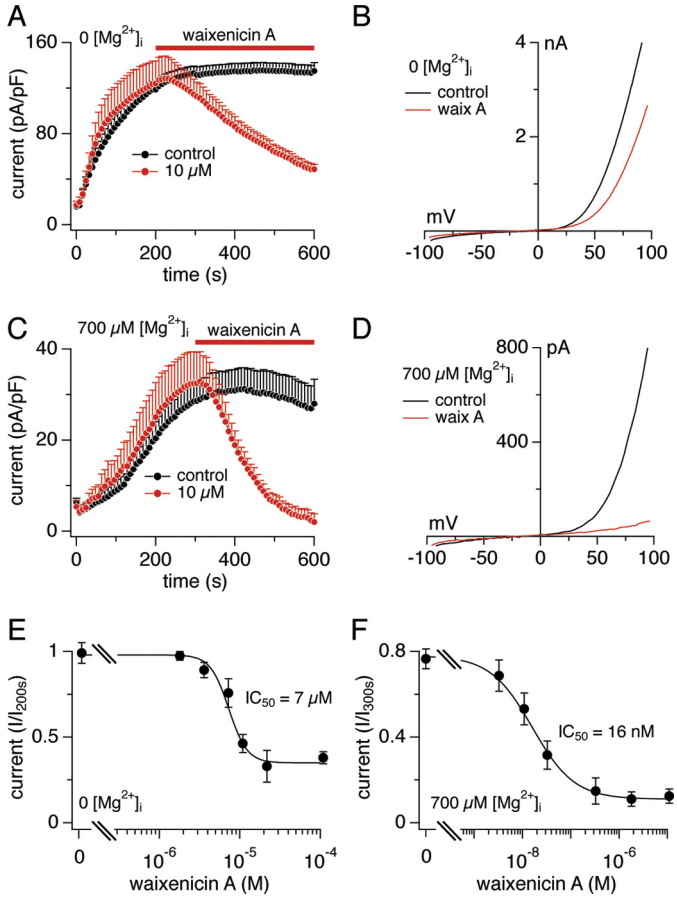

FIGURE 2. **Mg^{2+} dependence of waixenicin A block**. *Error bars* represent S.E. *A*, TRPM7 current densities in HEK293-TRPM7 without (*black*, $n = 8$) and with 10 μM waixenicin A (*red*, $n = 9$). *B*, *I/V* relationships are representative currents obtained at 500 s. *C*, TRPM7 current densities in the presence of 700 μM $[Mg^{2+}]_i$ without (*black*, $n = 10$) and with waixenicin A (*red*, $n = 8$). Same analysis as described in *A*. *D*, *I/V* relationships are representative currents obtained at 600 s. *E*, waixenicin A was applied as described in *A*. Currents were extracted at +80 mV at 500 s, normalized to current at 200 s, plotted against concentration, and approximated by dose-response fit ($n = 8$–10). *F*, waixenicin A was applied as described in *C*. Currents were extracted at +80 mV at 600 s, normalized to current at 300 s, and analyzed as described in *E* ($n = 5$–13).

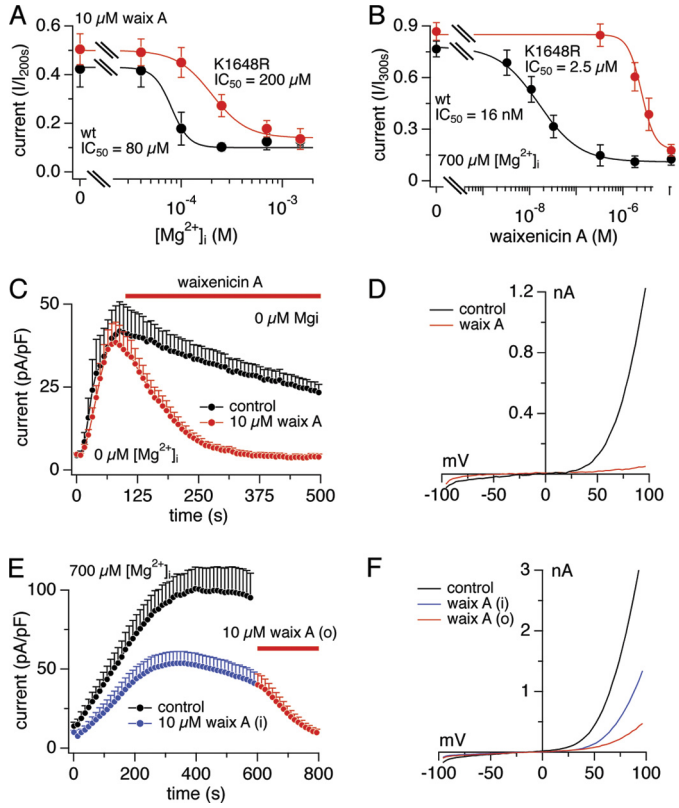

FIGURE 3. **Waixenicin A inhibits TRPM7 kinase domain mutants.** *Error bars* represent S.E. *A*, dose-response curve for $[Mg^{2+}]_i$ in waixenicin A-treated HEK293 cells overexpressing TRPM7-wt and TRPM7-K1648R. Current amplitudes at 600 s were normalized to maximal current, averaged, plotted against $[Mg^{2+}]_i$, and approximated by a dose-response fit ($n = 6$–10). *B*, data acquisition and analysis as in Fig. 2*C*. Normalized currents of TRPM7-wt cells (*black*) taken from Fig. 2*F* and TRPM7-K1648R cells (*red*) are plotted against concentration and approximated by dose-response fit ($n = 6$–9). *C*, TRPM7-ΔK current densities in zero $[Mg^{2+}]_i$ without (*black*, $n = 7$) and with 10 μM waixenicin A (*waix A*; *red*, $n = 8$). *D*, *I/V* relationships are representative currents obtained at 500 s. *E*, TRPM7-wt currents in the presence of 700 μM $[Mg^{2+}]_i$ without (*black*, $n = 17$) and with 10 μM waixenicin A applied first intracellularly (*blue*/*red*, $n = 14$) and then extracellularly (*red*, $n = 14$). *F*, *I/V* relationships are representative currents obtained at 600 s (*black* and *blue*) and 800 s (*red*).

Waixenicin A was also effective when applied intracellularly in TRPM7-overexpressing HEK293 cells with internal solution containing 700 μM Mg^{2+} and 10 μM waixenicin A, causing a ~50% reduction in current (Fig. 3, *E* and *F*). Reduced efficacy when applied through the patch pipette is not unexpected for a lipophilic compound due to diffusional escape of waixenicin A across the plasma membrane. Additional extracellular application of 10 μM waixenicin A completely suppressed the current. These results suggest that the primary site of action of waixenicin A is intracellular.

Waixenicin A Is a Relatively Specific TRPM7 Inhibitor—Although a few molecules have been reported to inhibit TRPM7, they all require micromolar concentrations, and none can be considered selective. We tested waixenicin A for selectivity against a panel of other cation channels, such as CRAC and members of the TRP superfamily, TRPM2, TRPM4, and the closest homolog of TRPM7, TRPM6. Although this is not an exhaustive panel of ion channels, they either are expressed in Jurkat and RBL cell lines we have studied in cell proliferation assays (see below) or are particularly interesting, as in the case of TRPM6, which has the highest homology to TRPM7.

The Ca^{2+}-permeable ion channel TRPM2 conducts monovalent and divalent cations (45–48). TRPM2 currents elicited by 100 μM adenosine-diphosphate ribose were recorded in HEK293 cells overexpressing TRPM2 (46). The application of 10 μM waixenicin A had no effect on TRPM2 current amplitudes or *I/V* relationships extracted before and after waixenicin A treatment (Fig. 4*A*).

TRPM4 is a Ca^{2+}-activated non-selective monovalent cation channel (49). TRPM4 currents were activated by 3 μM free internal Ca^{2+} in HEK293 cells overexpressing TRPM4 (49) and exposed to 10 μM waixenicin A. Both current amplitudes and *I/V* relationships remained unaffected by waixenicin A (Fig. 4*B*).

Because CRAC channels have similar pharmacological properties as TRPM7 (26, 28) and can be blocked by 2-aminoethyldiphenylborinate, La^{3+}, Gd^{3+}, and SKF-96365, we investigated the effect of 10 μM waixenicin A on native I_{CRAC}. CRAC currents elicited by 20 μM inositol 1,4,5-trisphosphate in RBL1 cells remained unaffected by waixenicin A (Fig. 4*C*).

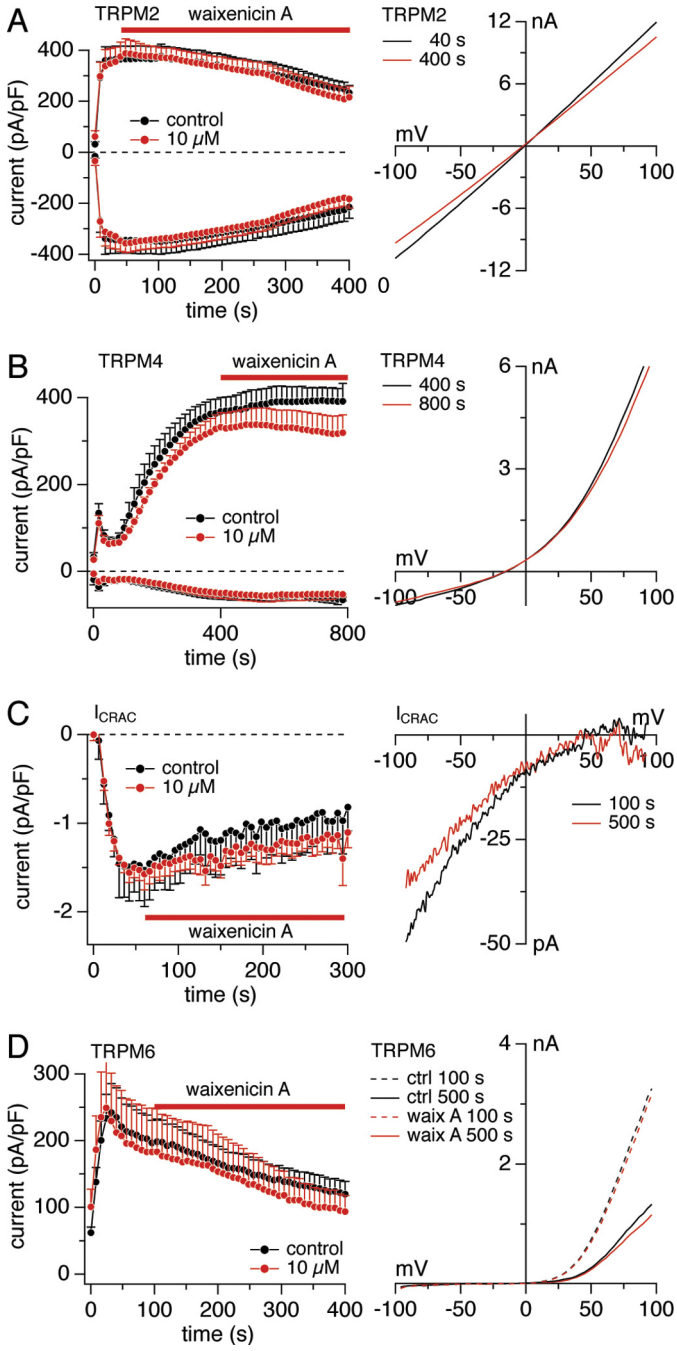

FIGURE 4. **Waixenicin A is specific for TRPM7**. *Error bars* represent S.E. *A*, current densities at −80/+80 mV elicited by 100 μM intracellular ADP-ribose in HEK293-TRPM2 cells without (*black*, $n = 6$) and with 10 μM waixenicin A (*red*, $n = 8$). Corresponding average *I/V* relationships in response obtained before (*black*, $n = 6$) and at the end of waixenicin A (*waix A*) application (*red*, $n = 8$). *B*, current densities at −80/+80 mV elicited by 3 μM $[Ca^{2+}]_i$ in HEK293-TRPM4 cells without (*black*, $n = 6$) and with 10 μM waixenicin A (*red*, $n = 7$). Corresponding *I/V* relationships are average currents obtained before (*black*, $n = 6$) and at the end of waixenicin A application (*red*, $n = 7$). *C*, native CRAC current densities at −80 mV elicited by 20 μM inositol 1,4,5-trisphosphate in RBL1 cells without (*black*, $n = 6$) and with 10 μM waixenicin A (*red circles*, $n = 6$). Corresponding *I/V* relationships are average currents obtained before (*black*, $n = 6$) and at the end of waixenicin A application (*red*, $n = 6$). *D*, current densities at +80 mV elicited by Mg^{2+}-free solution in HEK293-TRPM6 cells without (*black*, $n = 11$) and with 10 μM waixenicin A application (*red*, $n = 9$). *E*, representative *I/V* relationships extracted at 100 s (*dashed lines*) and 500 s (*solid lines*) from untreated controls (*ctrl*; *black*) and waixenicin A-treated cells (*red*).

TRPM6 is the closest subfamily relative of TRPM7, and they share similar permeation profiles and regulation by intracellular Mg^{2+} (4, 5, 50). We transfected HEK293 cells with TRPM6 and activated it with internal Mg^{2+}-free solution. Application of 10 μM waixenicin A did not alter TRPM6 current densities or I/V relationships compared with untreated controls (Fig. 4*D*). Unlike TRPM7, TRPM6 currents inactivated over time in both control and waixenicin A-treated cells. Taken together, our findings suggest that waixenicin A may indeed be relatively specific for TRPM7 as it does not significantly affect any other ion channels tested, including its closest homolog, TRPM6.

Waixenicin A Blocks Native TRPM7 Currents and Inhibits Cell Proliferation—We next investigated waixenicin A effects on native TRPM7. We used Jurkat T-cell lymphoma and RBL1 cells because these are the cell types in which native TRPM7 has been most extensively characterized, including biophysical channel characteristics, pharmacology, cell cycle, and involvement in cell proliferation and growth (2, 8, 20, 26, 27, 51). We perfused RBL1 cells with 0 or 700 μM intracellular free Mg^{2+} and exposed them to waixenicin A. In the absence of intracellular Mg^{2+}, native TRPM7 conductance was blocked partly by 10 μM waixenicin A and 300 nM waixenicin A had no effect (supplemental Fig. S3*A*). In the presence of 700 μM free intracellular Mg^{2+}, however, 300 nM waixenicin A was sufficient to completely block TRPM7 conductance (supplemental Fig. S3*B*). Increasing waixenicin A concentration to 10 μM accelerated inhibition of TRPM7 currents 2-fold, as determined by slope analysis (300 nM = −0.012 pA/pF/s *versus* 10 μM = −0.025 pA/pF/s).

Because TRPM7 has been implicated in cell growth and proliferation, we evaluated the proliferative activity of RBL1 cells incubated for 2 days with waixenicin A. Vital cell counts using trypan blue and mitochondrial dehydrogenase assays revealed a dose-dependent reduction in viable cell numbers (supplemental Figs. S4*A* and 5*A*) and observed that only at the highest concentration of 10 μM the number of dead cells increased (supplemental Fig. S4, *B* and *C*). We additionally performed annexin V/propidium iodide staining with subsequent flow cytometric analysis of RBL1 cells treated with waixenicin A for 2 days to assess apoptotic cell death (supplemental Fig. S5). Again, only the highest concentration of waixenicin A (10 μM) became toxic (Fig. 5*B* and supplemental Fig. S5*F*). Thus, the cell number reduction by waixenicin A below 10 μM was primarily due to inhibition of proliferation rather than toxicity.

Inhibition of proliferation by waixenicin A in intact cells revealed an IC_{50} in the low μM range (Fig. 5*A* and supplemental Fig. S4*A*), whereas in patch clamp experiments, it was in the nanomolar range (supplemental Fig. S3*B*). One explanation for this discrepancy could be the presence of serum proteins in growth assays (10% FBS). We performed cell cycle analysis using a BrdU/7-amino-actinomycin D assay to evaluate the impact of serum on waixenicin A activity. RBL1 cells were incubated in DMEM with or without 10% FBS and 3.3 μM waixenicin A was added 10 min before BrdU (Fig. 5, *C* and *D*). Cell populations slightly shifted along the *y* axis due to autofluorescence of waixenicin A (supplemental Fig. S6). The number of waixenicin A-treated cells in the S phase (for gating, see supplemental data) decreased by half (to 25.6 from 51.5% in control),

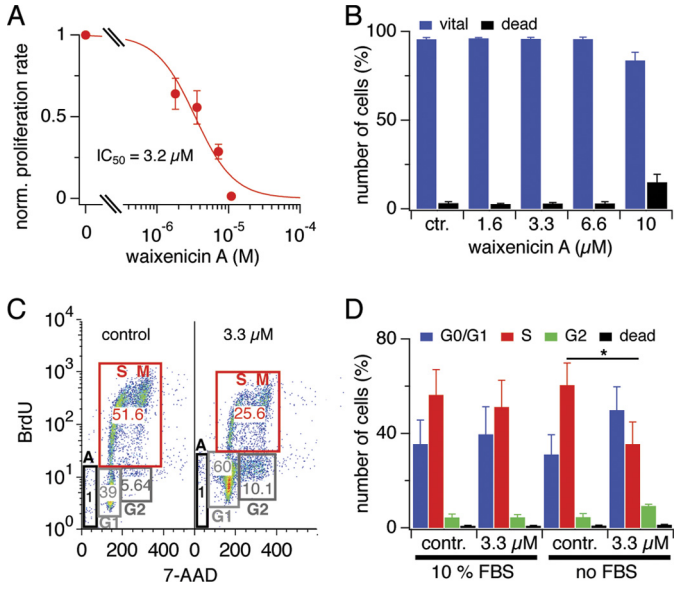

FIGURE 5. **Waixenicin A inhibits proliferation of RBL1 cells.** *Error bars* represent S.E. *A*, normalized proliferation rate of RBL1 cells treated with waixenicin A for 2 days and analyzed via MTT assay ($n = 3$). The absorbance ratio of untreated controls represents 100% of proliferation rate. *B*, RBL1 cells were treated as in *A*, stained with annexin V/phosphatidylinositol, and analyzed via flow cytometry. *Bars* represent normalized (*norm.*) cell numbers ($n = 3$). *C*, cell cycle analysis of RBL1 cells incubated with or without 10% FBS, 3.3 μM waixenicin A, and BrdU for 6 h. Cells were stained with antiBrdU antibody and 7-AAD and analyzed via flow cytometry. Representative plots of control (*contr.*) cells and cells treated with 3.3 μM waixenicin A. *D*, statistical analysis of data set described in *E*. *Bars* represent normalized cell numbers ($n = 3$).

whereas the number of cells in the G_1 and G_2 phase almost doubled (from 39 to 60% for G_1 and from 5.6 to 10.1% for G_2) (Fig. 5*C*). However, 3.3 μM waixenicin A in the presence of 10% FBS was not sufficient to block cells from entering the S phase ($p < 0.01$) (Fig. 5*D*). Thus, the efficacy of waixenicin A was significantly higher without serum than in its presence, indicating that serum may partially explain the difference in potency observed in proliferation *versus* patch clamp assays.

To further assess cell cycle progression, we investigated Jurkat T-cells and confirmed the dose-dependent inhibitory effect of waixenicin A (Fig. 6, *A* and *B*). Cells were treated with different concentrations of waixenicin A and exposed to BrdU for 2 h in media containing 10% FBS. Waixenicin A was more potent in Jurkat cells than in RBL1 cells, as 300 nM waixenicin A effectively prevented cells from entering S phase (26 *versus* 48% in control). Increasing its concentration to 3.3 μM decreased the amount of cells entering the S phase by half to 24%, and 10 μM waixenicin A completely abolished S phase progression. Although the number of Jurkat cells in the S phase decreased with increased waixenicin A concentration, the number of cells in the G_1 phase increased, demonstrating dose-dependent growth arrest (Fig. 6*B*). When using the same external solution as in patch clamp experiments, efficacy was further enhanced, and 3.3 μM waixenicin A completely blocked entry into S phase (Fig. 6*C*). Taken together, the results establish that waixenicin A selectively blocks heterologous and native TRPM7 currents, exhibits nanomolar potency in the presence of intracellular Mg^{2+}, and arrests cell growth and proliferation with low cytotoxicity in two different tumor cell lines.

DISCUSSION

TRPM7 is a ubiquitous Mg^{2+}- and Ca^{2+}-permeable channel vital for cellular Mg^{2+} homeostasis and crucial for cell survival (2, 19, 21). Targeted deletion of TRPM7 in DT40 chicken B-cells results in cell cycle arrest in G_1/G_0 phase and subsequent inhibition of cell proliferation (2, 8), and mice lacking the full-length protein (52) or just the kinase domain of TRPM7 die during early embryonic development (6). Suppressing TRPM7 expression in hippocampal neurons is neuroprotective, as it reduces ischemic cell death, preserves cell function, and prevents ischemia-induced deficits in memory (12). This is likely caused by decreases in TRPM7-mediated Ca^{2+} or Zn^{2+} influx (9, 11, 12). At present, there are only relatively unspecific blockers for TRPM7 that also affect other ion channels such as the CRAC channels (9, 26–28) or other TRP channel family members (29). A specific pharmacological approach that could be used to acutely and temporarily suppress TRPM7 function would provide better insights into the role of TRPM7 in malignant cell proliferation and neurotoxicity.

This study establishes waixenicin A, a xenicane diterpenoid from the Hawaiian soft coral *S. edmondsoni* with no previously reported activity (42), as a highly potent and selective inhibitor of the TRPM7 ion channel. A screening assay based on Mn^{2+} quenching of fura-2 (43) identified TRPM7 inhibitory activity for the soft coral extract and waixenicin A as the major active component of the extract, whereas patch clamp experiments confirmed waixenicin A as a TRPM7 antagonist. Additionally, it demonstrates that the pharmacological inhibition of TRPM7 by waixenicin A causes growth arrest in G_0/G_1 phase of the cell cycle.

The inhibitory effects of waixenicin A on TRPM7 are strongly dependent on the prevailing intracellular Mg^{2+} concentration. This further distinguishes the compound from other known pharmacological TRPM7 inhibitors, which are mostly nonspecific pore blockers and do not have a known Mg^{2+} dependence or nanomolar potencies (9, 26–28, 30). Mutational analysis involving the channel kinase domain and its previously identified Mg^{2+} binding site reveal a complex interaction of waixenicin A and Mg^{2+}. Under physiological conditions of 700 μM Mg^{2+}, waixenicin A inhibits TRPM7 with an IC_{50} of 16 nM, but its potency is greatly reduced when removing Mg^{2+}, resulting in an IC_{50} of just 7 μM. This indicates that waixenicin A and $[Mg^{2+}]_i$ synergize to inhibit the channel. The relevant Mg^{2+} binding site involved in this mechanism appears to be Lys-1648 within the kinase domain. This residue has been demonstrated to alter the sensitivity of the channel to intracellular Mg^{2+} and Mg-ATP (7, 8). In this study, we demonstrate that removing this Mg^{2+} binding site through mutation K1648R indeed caused a dramatic shift in the dose-response curve to waixenicin A from an IC_{50} of 16 nM in TRPM7-wt to 2.5 μM in the presence of physiological $[Mg^{2+}]_i$ levels of 700 μM. Because Mg^{2+} itself acts as an inhibitor of TRPM7, the synergy between waixenicin A and Mg^{2+} could be either due to waixenicin A-mediated enhancement of Mg^{2+} block or that Mg^{2+} enhances binding affinity of waixenicin A.

Although we have established an interaction between the Lys-1648 residue of the kinase domain and waixenicin A effects,

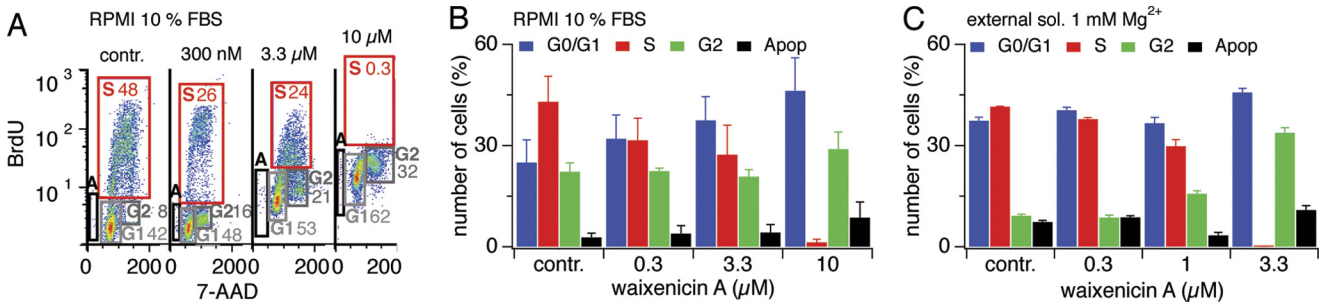

FIGURE 6. **Waixenicin A causes growth arrest in Jurkat T-cells.** *Error bars* represent S.E. *A*, cell cycle analysis of Jurkat cells incubated in RPMI media with 10% FBS and waixenicin A plus BrdU for 2 h ($n = 3$). Cells were stained with antiBrdU antibody and 7-AAD and analyzed via flow cytometry. *B*, statistical analysis of the data set as described in *A*. *Bars* represent normalized cell numbers ($n = 3$). *C*, Jurkat cells were incubated in standard external solution (*sol.*) containing 1 mM Mg^{2+} with no FBS. Different waixenicin A-concentrations were applied for 2 h, and cells were analyzed as described in *B*. *Bars* represent average cell numbers ($n = 3$). *Apop*, apoptotic cells.

the kinase deletion mutant TRPM7-ΔK suggests that waixenicin A does not necessarily bind to the kinase domain itself, as waixenicin A remains effective in blocking the channel even when the entire kinase domain is absent. In fact, waixenicin A is more potent and effective at blocking TRPM7-ΔK than either wild-type or K1648R channels and does so even in the complete absence of extra- and intracellular Mg^{2+}. This indicates that waixenicin A can bind to TRPM7 outside of the kinase domain with high affinity and block the channel independently of Mg^{2+} at least in TRPM7 truncation constructs. Although other interpretations cannot be ruled out, the following scenario would most adequately explain our observations: in the absence of Mg^{2+}, the TRPM7-wt channel has a low affinity to waixenicin A because the binding site of the compound is partly masked. At physiological Mg^{2+} levels, when the Lys-1648 residue is occupied with Mg^{2+}, TRPM7 will be in a conformational state that enables waixenicin A to bind with high affinity and effectively block the channel. Thus, the synergy between waixenicin A and Mg^{2+} appears to be caused by a change in affinity of TRPM7 for waixenicin A rather than enhancement of Mg^{2+} block. Removing the entire kinase domain exposes the waixenicin A binding site so that waixenicin A can bind with high affinity and block TRPM7 largely independently of Mg^{2+}.

Waixenicin A suppressed cell growth in various proliferation assays of RBL1 and Jurkat T-cells, complementing previous observations that TRPM7-deficient cells fail to grow and proliferate (20). Waixenicin A induced a dose-dependent reduction of cells in synthesis phase and an accumulation of cells in G_0/G_1 and G_2 phase of the cell cycle. This suggests that the G_1/S as well as the G_2/M transition is impaired. It has been shown that TRPM7-deficient cells exhibit substantially decreased signaling along the PI3K pathway (20). A key effector in this pathway is protein kinase B (or Akt). Constitutive protein kinase B expression was not sufficient to support TRPM7-independent growth, whereas PI3K expression was sufficient (20). The PI3K pathway is activated during G_1/S transition, and PI3K is required for G_1/S phase progression in lymphocytes. In particular, PI3K activation is linked to restriction point progression and coincides with G_1 events that cumulate in cyclin E/cyclin-dependent kinase-2 activation. Thus, PI3K pathway activation is required for G_1/S progression and PI3K inhibition leads to G_1 arrest in many cell types (reviewed in Ref. 53). Moreover, the PI3K/protein kinase B pathway may also regulate the efficiency of G_2/M phase progression (54), suggesting cross-talk between the PI3K pathway and key regulators of DNA damage checkpoint machinery. It is therefore not surprising that we find fewer cells in S phase, whereas the numbers of cells in G_1/G_0 and G_2 phase increase during waixenicin A treatment. Thus, our data suggest that blocking TRPM7 conductance, resulting in failure of G_1/S and G_2/M progression, might also negatively affect the PI3K/protein kinase B pathway as previously shown for TRPM7 knock-out DT40 cells (20).

We found that waixenicin was less potent in long term cell growth assays (low micromolar range) compared with acute inhibitory effects observed in patch clamp experiments (low nanomolar range). Possible factors that might contribute to this discrepancy include cellular sequestration of the waixenicin A, conversion into inactive metabolites, up-regulation of compensatory Mg^{2+} transport mechanisms that counteract the lowered Mg^{2+} transport via TRPM7, and/or reduced bioavailability of waixenicin due to serum binding. Indeed, we found that waixenicin A was less potent in the presence of serum, indicating direct binding of waixenicin A to serum proteins, and thereby effectively lowering free waixenicin A concentration. Moreover, serum and growth factors in the medium may activate additional mitogenic signals such as cyclin-dependent kinases, which contribute to cell cycle progression and might offset the inhibition by waixenicin A. Proliferative signals can also be transduced by proto-oncogenes, even in the face of reduced or absent growth factors. Constitutive oncogene activation plays a key role in carcinogenesis and tumor progression. Because constitutive or increased activity of PI3K-dependent pathways present a major means whereby tumor cells achieve uncontrolled proliferation (53), waixenicin A might be particularly effective in targeting oncogenic cell growth. Additionally, tumor cells accumulate Mg^{2+} at the expense of surrounding cells, and waixenicin A is much more potent in inhibiting TRPM7 conductance in the presence of elevated intracellular Mg^{2+}. Thus, waixenicin A represents a novel natural compound with anti-proliferative activity, whose mechanism is based on a highly potent and seemingly specific inhibition of Mg^{2+} transport via TRPM7.

We confirmed the specificity of waixenicin A against a number of ion channels found in our cellular model systems of Jurkat and RBL cells, including ICRAC, TRPM2, TRPM4, and TRPM6. Although we cannot rule out potential effects on other channels or proteins, we consider the specificity of TRPM7 as relatively high for the following reasons: (i) blocking efficacy

occurs in the low nanomolar range, (ii) this potency is dependent on Mg^{2+} binding at a strategic residue, Lys-1648, in the kinase domain of TRPM7, (iii) TRPM6, the only other known channel kinase and the most homologous relative of TRPM7 within the TRPM subfamily, remained unaffected by the waixenicin A even at 10 μM. These features make waixenicin A an attractive molecular structure for targeting TRPM7-related pathophysiologies such as cancer (18, 19, 21), ischemia-related neuronal death (10, 11), and cardiac fibrosis and atrial fibrillations (55–57), and they open the door to future structure activity relationship studies of the waixencin A pharmacophore. Such studies would be aimed at elucidating the structural features of waixencin A that are essential for TRPM7 inhibition and making modifications to improve solubility and/or bioavailability. It might also be possible to reduce and/or simplify the structure to facilitate synthetic chemistry of analogs.

Acknowledgments—We thank L. Tsue, S. Johne, and M. K. Monteilh-Zoller for technical support, Dr. R. J. M. Bindels for the TRPM6 plasmid, and Dr. S. Kahng for soft coral identification.

REFERENCES

1. Li, M., Jiang, J., and Yue, L. (2006) *J. Gen. Physiol.* **127,** 525–537
2. Nadler, M. J., Hermosura, M. C., Inabe, K., Perraud, A. L., Zhu, Q., Stokes, A. J., Kurosaki, T., Kinet, J. P., Penner, R., Scharenberg, A. M., and Fleig, A. (2001) *Nature* **411,** 590–595
3. Ryazanova, L. V., Dorovkov, M. V., Ansari, A., and Ryazanov, A. G. (2004) *J. Biol. Chem.* **279,** 3708–3716
4. Chubanov, V., Gudermann, T., and Schlingmann, K. P. (2005) *Pflugers Arch.* **451,** 228–234
5. Voets, T., Nilius, B., Hoefs, S., van der Kemp, A. W., Droogmans, G., Bindels, R. J., and Hoenderop, J. G. (2004) *J. Biol. Chem.* **279,** 19–25
6. Ryazanova, L. V., Rondon, L. J., Zierler, S., Hu, Z., Galli, J., Yamaguchi, T. P., Mazur, A., Fleig, A., and Ryazanov, A. G. (2010) *Nat. Commun.* **1,** 109
7. Demeuse, P., Penner, R., and Fleig, A. (2006) *J. Gen. Physiol.* **127,** 421–434
8. Schmitz, C., Perraud, A. L., Johnson, C. O., Inabe, K., Smith, M. K., Penner, R., Kurosaki, T., Fleig, A., and Scharenberg, A. M. (2003) *Cell* **114,** 191–200
9. Monteilh-Zoller, M. K., Hermosura, M. C., Nadler, M. J., Scharenberg, A. M., Penner, R., and Fleig, A. (2003) *J. Gen. Physiol.* **121,** 49–60
10. Aarts, M., Iihara, K., Wei, W. L., Xiong, Z. G., Arundine, M., Cerwinski, W., MacDonald, J. F., and Tymianski, M. (2003) *Cell* **115,** 863–877
11. Inoue, K., Branigan, D., and Xiong, Z. G. (2010) *J. Biol. Chem.* **285,** 7430–7439
12. Sun, H. S., Jackson, M. F., Martin, L. J., Jansen, K., Teves, L., Cui, H., Kiyonaka, S., Mori, Y., Jones, M., Forder, J. P., Golde, T. E., Orser, B. A., Macdonald, J. F., and Tymianski, M. (2009) *Nat. Neurosci.* **12,** 1300–1307
13. Nicotera, P., and Bano, D. (2003) *Cell* **115,** 768–770
14. Szydlowska, K., and Tymianski, M. (2010) *Cell Calcium* **47,** 122–129
15. Tseveleki, V., Rubio, R., Vamvakas, S. S., White, J., Taoufik, E., Petit, E., Quackenbush, J., and Probert, L. (2010) *Genomics* **96,** 82–91
16. Abed, E., and Moreau, R. (2007) *Cell Prolif.* **40,** 849–865
17. Abed, E., and Moreau, R. (2009) *Am. J. Physiol. Cell Physiol.* **297,** C360–368
18. Guilbert, A., Gautier, M., Dhennin-Duthille, I., Haren, N., Sevestre, H., and Ouadid-Ahidouch, H. (2009) *Am. J. Physiol. Cell Physiol.* **297,** C493–502
19. Jiang, J., Li, M. H., Inoue, K., Chu, X. P., Seeds, J., and Xiong, Z. G. (2007) *Cancer Res.* **67,** 10929–10938
20. Sahni, J., and Scharenberg, A. M. (2008) *Cell Metab.* **8,** 84–93
21. Kim, B. J., Park, E. J., Lee, J. H., Jeon, J. H., Kim, S. J., and So, I. (2008) *Cancer Sci.* **99,** 2502–2509
22. Wykes, R. C., Lee, M., Duffy, S. M., Yang, W., Seward, E. P., and Bradding, P. (2007) *J. Immunol.* **179,** 4045–4052
23. Wolf, F. I., Trapani, V., and Cittadini, A. (2008) *Magnes. Res.* **21,** 83–91
24. Wolf, F. I., Cittadini, A. R., and Maier, J. A. (2009) *Cancer Treat Rev.* **35,** 378–382
25. Chen, J. P., Luan, Y., You, C. X., Chen, X. H., Luo, R. C., and Li, R. (2010) *Cell Calcium* **47,** 425–432
26. Hermosura, M. C., Monteilh-Zoller, M. K., Scharenberg, A. M., Penner, R., and Fleig, A. (2002) *J. Physiol.* **539,** 445–458
27. Kerschbaum, H. H., Kozak, J. A., and Cahalan, M. D. (2003) *Biophys. J.* **84,** 2293–2305
28. Kozak, J. A., Kerschbaum, H. H., and Cahalan, M. D. (2002) *J. Gen. Physiol.* **120,** 221–235
29. Parnas, M., Peters, M., Dadon, D., Lev, S., Vertkin, I., Slutsky, I., and Minke, B. (2009) *Cell Calcium* **45,** 300–309
30. Chen, H. C., Xie, J., Zhang, Z., Su, L. T., Yue, L., and Runnels, L. W. (2010) *PLoS One* **5,** e11161
31. Peinelt, C., Lis, A., Beck, A., Fleig, A., and Penner, R. (2008) *J. Physiol.* **586,** 3061–3073
32. Zhang, S. L., Kozak, J. A., Jiang, W., Yeromin, A. V., Chen, J., Yu, Y., Penna, A., Shen, W., Chi, V., and Cahalan, M. D. (2008) *J. Biol. Chem.* **283,** 17662–17671
33. DeHaven, W. I., Smyth, J. T., Boyles, R. R., Bird, G. S., and Putney, J. W., Jr. (2008) *J. Biol. Chem.* **283,** 19265–19273
34. Matsuda, H., Hayashi, M., and Okada, M. (2010) *J. Physiol.* **588,** 4673–4681
35. Li, M., Sun, Y., Simard, J. M., Wang, J. Y., and Chai, T. C. (2009) *Am. J. Physiol. Cell Physiol.* **297,** C1445–1451
36. Kucherenko, Y. V., and Lang, F. (2010) *J. Membr. Biol.* **237,** 93–106
37. Coburn, R. F. (2009) *J. Cell. Physiol.* **221,** 544–551
38. Mastrocola, T., De Luca, M., and Rugolo, M. (1991) *Biochim. Biophys. Acta* **1097,** 275–282
39. Korn, S. J., and Horn, R. (1990) *Mol. Pharmacol.* **38,** 524–530
40. Hatton, C. J., and Peers, C. (1997) *Br. J. Pharmacol.* **122,** 923–929
41. Gong, Y. Z., Ding, W. G., Wu, J., Tsuji, K., Horie, M., and Matsuura, H. (2008) *Eur. J. Pharmacol.* **600,** 18–25
42. Coval, S., Scheuer P., Matsumoto G., and Clardy J. (1984) *Tetrahedron* **40,** 3823
43. Castillo, B., Pörzgen, P., Penner, R., Horgen, F. D., and Fleig, A. (2010) *J. Biomol. Screen* **15,** 498–507
44. Lang, G., Mitova, M. I., Ellis, G., van der Sar, S., Phipps, R. K., Blunt, J. W., Cummings, N. J., Cole, A. L., and Munro, M. H. (2006) *J. Nat. Prod.* **69,** 621–624
45. Lange, I., Yamamoto, S., Partida-Sanchez, S., Mori, Y., Fleig, A., and Penner, R. (2009) *Sci. Signal* **2,** ra23
46. Perraud, A. L., Fleig, A., Dunn, C. A., Bagley, L. A., Launay, P., Schmitz, C., Stokes, A. J., Zhu, Q., Bessman, M. J., Penner, R., Kinet, J. P., and Scharenberg, A. M. (2001) *Nature* **411,** 595–599
47. Starkus, J. G., Fleig, A., and Penner, R. (2010) *J. Physiol.* **588,** 1227–1240
48. Yamamoto, S., Shimizu, S., Kiyonaka, S., Takahashi, N., Wajima, T., Hara, Y., Negoro, T., Hiroi, T., Kiuchi, Y., Okada, T., Kaneko, S., Lange, I., Fleig, A., Penner, R., Nishi, M., Takeshima, H., and Mori, Y. (2008) *Nat. Med.* **14,** 738–747
49. Launay, P., Fleig, A., Perraud, A. L., Scharenberg, A. M., Penner, R., and Kinet, J. P. (2002) *Cell* **109,** 397–407
50. Cao, G., Hoenderop, J. G., and Bindels, R. J. (2008) *Curr. Opin. Nephrol. Hypertens* **17,** 373–378
51. Tani, D., Monteilh-Zoller, M. K., Fleig, A., and Penner, R. (2007) *Cell Calcium* **41,** 249–260
52. Jin, J., Desai, B. N., Navarro, B., Donovan, A., Andrews, N. C., and Clapham, D. E. (2008) *Science* **322,** 756–760
53. Liang, J., and Slingerland, J. M. (2003) *Cell Cycle* **2,** 339–345
54. Shtivelman, E., Sussman, J., and Stokoe, D. (2002) *Curr. Biol.* **12,** 919–924
55. Du, J., Xie, J., Zhang, Z., Tsujikawa, H., Fusco, D., Silverman, D., Liang, B., and Yue, L. (2010) *Circ. Res.* **106,** 992–1003
56. Sontia, B., Montezano, A. C., Paravicini, T., Tabet, F., and Touyz, R. M. (2008) *Hypertension* **51,** 915–921
57. Yue, L., Xie, J., and Nattel, S. (2011) *Cardiovasc. Res.* **89,** 744–753

Supporting Information (SI)

WAIXENICIN A INHIBITS CELL PROLIFERATION THROUGH MAGNESIUM-DEPENDENT BLOCK OF TRPM7

Susanna Zierler[1,3], Guangmin Yao[2,4], Zheng Zhang[1], W. Cedric Kuo[2], Peter Pörzgen[2], Reinhold Penner[1], F. David Horgen[2] and Andrea Fleig[1]

[1]*Center for Biomedical Research, The Queen's Medical Center and John A. Burns School of Medicine, University of Hawaii, Honolulu, Hawaii 96813, U.S.A.*

[2]*Laboratory of Marine Biological Chemistry, Department of Natural Sciences, Hawaii Pacific University, Kaneohe, HI 96744, U.S.A.*

[3] *Present address: Walther-Straub-Institute for Pharmacology and Toxicology, Ludwig-Maximilians-University Munich, 80336 Munich, Germany*

[4] *Present address: School of Pharmacy, Tongji Medical College, Huazhong University of Science and Technology,13 Hangkong Road, Wuhan, 430030, P.R. China*

SUPPLEMENTAL PROCEDURES

Animal material

The soft coral *S. edmondsoni* was collected in waters adjacent to Lanikai Beach, on the island of Oahu. Samples were immediately frozen at –20 °C and then freeze-dried. The soft coral was identified as *Sarcothelia edmondsoni* (formerly known as *Anthelia edmondsoni*). The freeze-dried sample (325 mg dry wt) was extracted twice with methanol (11 ml), and solvent was removed from the combined extracts under vacuum to yield 117 mg of extract residue. Prior to assay, the extract was redissolved in methanol/ethyl acetate/*t*-butyl methyl ether (60:30:10) (MET) and diluted in Krebs-Ringer-HEPES (KRH) buffer (135 mM NaCl, 5 mM KCl, 1.5 mM $MgCl_2$, 1.5 mM $CaCl_2$, and 20 mM HEPES, and 5.6 mM glucose). The extract was tested for inhibitory effects on TRPM7-mediated cation flux in a fluorescence-based assay in duplicate on separate days at a concentration of 30 µg/ml (2% MET).

Fluorescence-based TRPM7 bioassay

The *S. edmondsoni* extract, its fractions, and isolated waixenicin-A (Fig. 1E) were assayed against TRPM7 using a previously reported (32) high-throughput bioassay system, that measures TRPM7-mediated Mn^{2+} influx via fluorescence quench of fura-2 calcium imaging dye in a TRPM7-overexpressing HEK293 cell line (2). In brief, HEK293-TRPM7 cells (50,000-60,000 cells/well) were plated in poly-L-lysine coated 96-well plates and TRPM7-expression was induced 2-3 hr post plating by the addition of 2 μg/ml tetracycline. The culture medium was completely removed at 18 hr post induction and replaced with fura-2 loading-buffer: 2 mM fura-2-acetoxymethyl ester (Invitrogen), 2 mM probenecid (Sigma), and 0.3% pluronic F-127 (Sigma) in KRH. Following incubation (45 min at 37 °C), the loading buffer was removed, and the cells were washed once with KRH before addition of fresh KRH as the assay buffer. The plates were then transferred to a pre-warmed (37 °C) FlexStation (Molecular Devices) fluorescence plate reader. Cells were initially incubated with test substances or vehicle for ~15 min. Vehicle-receiving, induced TRPM7-HEK293 cells served as positive control for the activation of a TRPM7-mediated Mn^{2+}-influx, while wells containing parental HEK293 cells (receiving vehicle) served as negative controls to define the background for the changes of cytosolic $[Mn^{2+}]$. The Ca^{2+}-independent fluorescence (excitation 360 nm; emission 510 nm) of fura-2 was monitored following the addition of 10 mM $MnCl_2$. The TRPM7-mediated increase in $[Mn^{2+}]_i$ was processed in SoftMax Pro (v 5.3, Molecular Devices) as the maximum slope of fluorescence change after $MnCl_2$ addition, and the data was background corrected and normalized by expressing sample-treated well maximum slope as a percent of vehicle-control. For dose-response determination, IC_{50} values were determined from dose-response curves fitted in Igor Pro (Wavemetrics) by constraining the top of the curve (no inhibition) to 100% vehicle control.

Bioassay-linked fractionation of the S. edmondsoni organic extract

The active extract was fractionated by semi-preparative reversed-phase HPLC (Agilent 1100 binary liquid chromatograph; Phenomenex Luna C18-2 column, 5 µm, 10 x 250 mm) using a linear gradient of

acetonitrile/aqueous 10 mM ammonium acetate (23-68% acetonitrile over 0-2 min, 68-95% acetonitrile over 2-25 min, 95% acetonitrile over 25-40 min; flow rate: 3.8 ml/min; UV detection: 220-240 nm). Extract components eluting between 5-40 min were collected as 30-sec fractions into a deep 96-well plate. Solvent and buffer was removed from the plate under vacuum in a centrifugal concentrator at room temperature and fractions were reconstituted with MET and apportioned into low-profile 96-well plates for bioassay and chemical analysis. Prior to assay, the fractions were reconstituted with MET and diluted with KRH. Fractions were tested at an average concentration of 15 mg/ml, and data was pooled from single replicates tested on separate days.

Isolation of waixenicin-A

The scaled-up fractionation of the soft coral extract was guided by characteristic LC-MS data (electrospray ionization; ion trap analyzer; Thermo Finnigan LCQ Deca XP) obtained for the extract peak corresponding to the highest TRPM7 activity. Initially, the extract was subjected to vacuum liquid chromatography (stationary phase: silica; mobile phase: dichloromethane/methanol mixtures). The fraction eluting with dichloromethane/methanol (95:5) concentrated the targeted compound. Repeated semi-preparative reversed phase HPLC led to the isolation of waixenicin-A (Fig. 1E), which was identified by comparison of NMR data and optical rotation with literature values (34). The purity of our waixenicin-A sample was determined to be >95% based on LC-MS-evaporative light scattering detector (ELSD) analyses (Phenomenex Luna C18-2 column, 5 µm, 2 x 250 mm; mobile phase: linear gradient of acetonitrile/aqueous 10 mM ammonium acetate (50-100% acetonitrile over 0-50 min); Sedex 75 ELSD, 50 °C). For further physiological experiments, 25 µg of purified and lyophilized waixenicin-A was dissolved in 60 µl of methanol, diluted in the adequate buffer solution used for the subsequent experiments (100 µM stock solution) and stored at –20 °C.

Cell culture

A tetracycline-inducible HEK293 cell line overexpressing TRPM7 (2) was used for the fluorescence-based TRPM7 bioassay. For additional electrophysiological studies we used HEK293 cells transiently overexpressing TRPM7 (2) and TRPM7 mutants (6), TRPM2 (36) or TRPM4 (39), as well as rat basophilic leukemia (RBL1), RBL1-wt cells, and finally HEK293-wt cells transfected with a TRPM6 plasmid (kindly provided by Dr. Bindels). RBL1 cells and a human T-lymphocyte cell line (Jurkat) were used for proliferation, cell cycle and toxicity assays.

Electrophysiology

Patch-clamp experiments were performed in whole-cell configuration. High-resolution currents were acquired and recorded using EPC9 (HEKA) and PatchMaster (HEKA). All voltages were corrected for a liquid junction potential of 10 mV. Currents were elicited by a ramp protocol from –100 mV to +100 mV (TRPM7, I_{CRAC}) or –150 to +150 mV (TRPM2, TRPM4) over 50 ms acquired at 0.5 Hz and a holding potential of 0 mV. Inward current amplitudes were extracted at –80 mV, outward currents at +80 mV and plotted versus time of the experiment. Data were normalized to cell size as pA/pF. Standard extracellular solution contained (in mM): 140 NaCl, 1 $CaCl_2$, 2.8 KCl, 2 $MgCl_2$, 10 HEPES-NaOH, 11 Gluc (pH 7.2, 300 mOsm). Standard intracellular solution contained (in mM): 140 Cs-glutamate, 8 NaCl, 1 $MgCl_2$, 10 HEPES (pH 7.2, 300 mOsm). Mg-free intracellular solution contained (in mM): 120 Cs-glutamate, 8 NaCl, 10 HEPES, 10 Cs-BAPTA, 5 Na-EDTA (pH 7.2, 300 mOsm). For Mg^{2+} dose-response assessment intracellular solution contained (in mM): 140 Cs-glutamate, 8 NaCl, 10 Cs-BAPTA plus appropriate amounts of $MgCl_2$, as calculated with WebMaxC.

Proliferation and apoptosis assays

Cells were seeded at a density of 10^4 cells/ml in DMEM supplemented with 10% FBS and allowed to attach before waixenicin-A was added. Cell culture plates were incubated in a humidified incubator at 37 °C for two days.

ViCell Analysis: A Beckman Coulter ViCell Automated Cell Viability Analyzer (Beckman Coulter, Inc., Brea, CA) was used to stain RBL1 cells with trypan blue and count all live and dead cells of 100 digital

images. Total number of vital cells was normalized to the untreated control. Cells that were stained with trypan blue were considered as dead cells and normalized to the total amount of cells in the sample.

MTT-assay: Part of the media was removed and 50 µl of 5 mg/ml thiazolyl blue tetrazolium bromide (MTT, Sigma) was added to the remaining 500 µl of media. Cells were incubated for 3 h at 37 °C until purple crystals formed. Finally, 500 µl of MTT solvent (0.1 N HCl in isopropanol) were added and after the crystals dissolved, the absorbance ratio A/R (with A = 540 nm and R = 630 nm) was read using a Benchmark Plus microplate spectrophotometer (Bio-Rad). Experiments were made in triplets.

Annexin-V–propidium iodide assay: A modified annexin-V-FITC Apoptosis Detection Kit (Sigma) was used to determine the percentage of apoptotic cells. Cells were collected in centrifuge tubes using Trypsin/EDTA and centrifuged at 1000 rpm for 7 min. The supernatant was removed and cells were resuspended in 300 µl of 1 x binding buffer (Sigma). Thereafter, 7 µl of propidium iodide (PI) and 10 µl of FITC-conjugated anti-Annexin-V antibody (Sigma) were added and incubated for 15 min. Finally, cells were analyzed using a fluorescence activated cell sorter (FACS Calibur, BD Biosciences).

Cell cycle analysis

For cell cycle analysis, a FITC BrdU Flow Kit (BD Pharmingen) was used according to manufacturer's instructions. In brief, cells were seeded at a density of 0.5 x 10^6 cells/ml and allowed to equilibrate for 10 min before waixenicin-A was added. Subsequently, cells were incubated for another 15 min before BrdU was added. After another 2-6 hours of incubation time, the cells were fixed and permealized. Thereafter, DNase was added to expose the BrdU epitopes, which were stained using a FITC conjugated anti-BrdU antibody while the DNA content was stained using 7-AAD. Cells were analyzed via flow cytometry (FACS, BD Biosciences) with excitation of 488 nm and FL-1 emission of 530 nm (bandpass filter) for FITC-conjugated anti-BrdU antibody detection and FL-3 emission of >670 nm (bandpass filter) for 7-AAD detection. The upper gate represents all cells that have incorporated BrdU, including cells in the synthesis (S) and mitosis (M) phase of the cell cycle. The lower left gate represents dead cells and apoptotic cell debris (A). The middle lower gate shows cells in G1/G0-phase of the cell cycle (G1) where they have a normal DNA pool (2 n), whereas the right lower gate represents cells that have already doubled their DNA content (4 n) and are in G2-phase of the cell cycle (G2).

Statistical analysis

Unless stated otherwise, data represent the mean of individual experiments ±standard error of mean (S.E.M.). An unpaired student's t-test was applied for significance analysis and $P<0.05$ was considered statistically significant.

SUPPLEMENTAL FIGURES AND LEGENDS

Fig. S1. Waixenicin-A affects outward and inward currents similarly
Fig. S2. Waixenicin-A and extracellular Mg^{2+} in TRPM7-wt and TRPM7-ΔK
Fig. S3. Waixenicin-A blocks native TRPM7 currents.
Fig. S4. Waixenicin-A dose-dependently inhibits proliferation without being toxic
Fig. S5. Toxicity of waixenicin-A is above 10 µM
Fig. S6. Waixenicin-A-treated cells exhibit green auto-fluorescence at 488 nm laser excitation

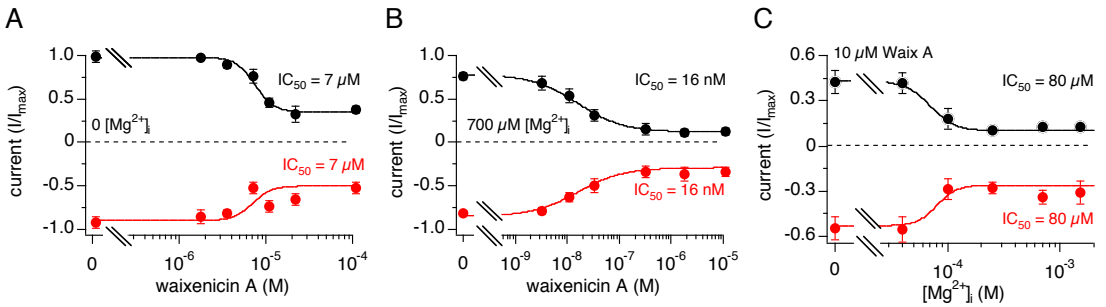

Fig. S1. Waixenicin-A affects outward and inward currents similarly. A. Same data set as in Fig. 2E. Different concentrations of waixenicin-A were applied as shown in Fig. 2A. Currents were extracted at +80 mV (black) and –80 mV (red) at 500 s, normalized to the maximal current amplitude before application (200 s), averaged, plotted against waixenicin-A concentration and approximated by a dose-response fit function (n = 8-10). *B.* Same data set as in Fig. 2F. Different concentrations of waixenicin-A were applied as shown in Fig. 2C. Currents were extracted at +80 mV (black) and –80 mV (red) at 600 s, normalized to the maximal current amplitude before application (300 s), averaged, plotted against waixenicin-A concentration and approximated by a dose-response fit function (n = 5-13). *C.* Same data set as in Fig. 3A for TRPM7-wt. Application solution contained 10 μM waixenicin-A. Currents were extracted at +80 mV (black) and –80 mV (red) at 600 s, normalized to the maximal current amplitude before application, averaged, plotted against $[Mg^{2+}]_i$ and approximated by a dose-response fit function (see Methods; n = 6-10). Note that inward and outward currents reveal the same IC_{50} and Hill coefficients for all conditions. Error bars represent S.E.M.

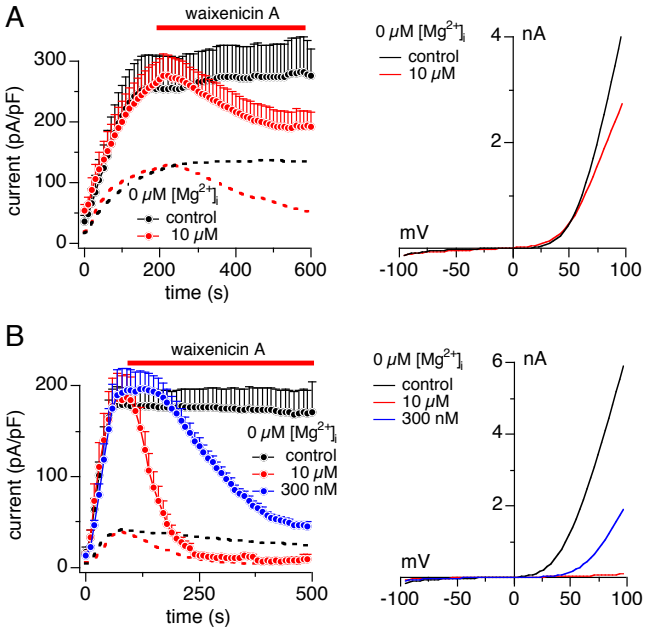

Fig. S2. Waixenicin-A and extracellular Mg2+ in TRPM7-wt and TRPM7-ΔK. A. Currents in HEK293 cells overexpressing TRPM7-wt were recorded in the absence of extracellular Mg^{2+} and normalized to cell size without (black, n = 12) and with 10 μM waixenicin-A application (red, n = 12). The dotted lines represent the same data set as in *Fig. 2A* in the presence of extracellular Mg^{2+}. Error bars represent S.E.M. Corresponding I/V relationships are representative currents in response to voltage ramps obtained at 500 s into the experiment. The external solution contained nominally zero Mg^{2+} (in mM: 140 NaCl, 1 $CaCl_2$, 2.8 KCl, 10 HEPES-NaOH, 11 Gluc). *B.* Time course of TRPM7-ΔK currents normalized to cell size without (black, n = 9) and with 10 μM (red, n = 10) or 300 nM (blue, n = 8) waixenicin-A application. Experimental conditions were the same as in *A*. The dotted lines represent the same data set as in *Fig. 3C* in the presence of extracellular Mg^{2+}. Error bars represent S.E.M. Corresponding I/V relationships are representative currents in response to voltage ramps obtained at 400 s into the experiment.

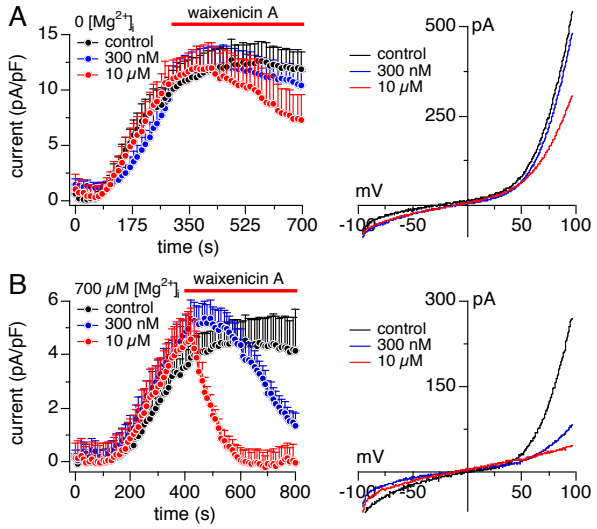

Fig. S3. Waixenicin-A blocks native TRPM7 currents. A. Normalized native TRPM7 currents at +80 mV in RBL cells without (black, n = 8) and with 300 nM (blue, n = 8) or 10 µM (red, n = 8) waixenicin-A application. TRPM7 currents were elicited by intracellular zero Mg^{2+}. Corresponding I/V relationships are average currents in response to voltage ramps obtained at 700 s in untreated controls (black, n = 5) and 300 nM (blue, n = 4) or 10 µM waixenicin-A (red, n = 5). *B.* Same experimental protocol as in *A*, except that intracellular free Mg^{2+} was clamped to 700 µM. Normalized native TRPM7 currents at +80 mV without (black circles, n = 7) and with 300 nM (blue, n = 9) or 10 µM waixenicin-A (red, n = 5). Corresponding I/V relationships are average currents in response to voltage ramps obtained at 800 s in untreated controls (black, n = 3) and 300 nM (blue, n = 3) or 10 µM waixenicin-A (red, n = 3). Error bars represent S.E.M.

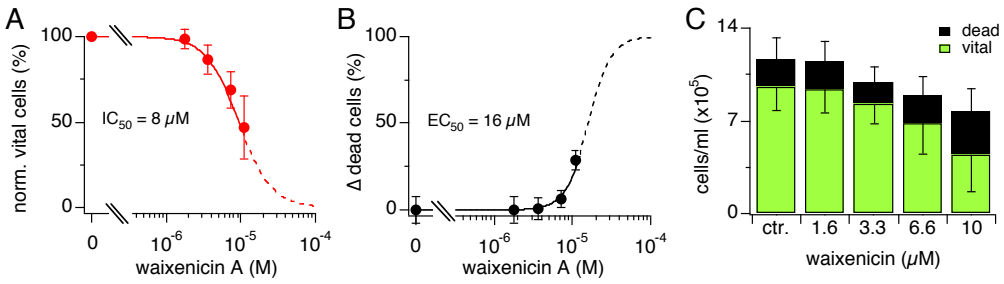

Fig. S4. Waixenicin-A dose-dependently inhibits proliferation without being toxic. A. Trypan blue staining of RBL1 cells treated with different concentrations of waixenicin-A for 2 days. Cells were analyzed via a VICell counter screening 100 individual images (n = 3). Relative numbers of unstained cells were averaged, normalized to the untreated control and plotted against waixenicin-A concentration. Error bars represent S.E.M. *B.* Trypan blue positive cells were analyzed from the same data set as in *A*. Relative numbers of dead cells were averaged and plotted against waixenicin-A concentration. Error bars represent S.E.M. *C.* Total cell count of trypan blue-stained cells per ml. Raw data are represented as mean of three independent experiments. Error bars indicate S.E.M. Note a reduction in total cell number with increasing compound concentrations.

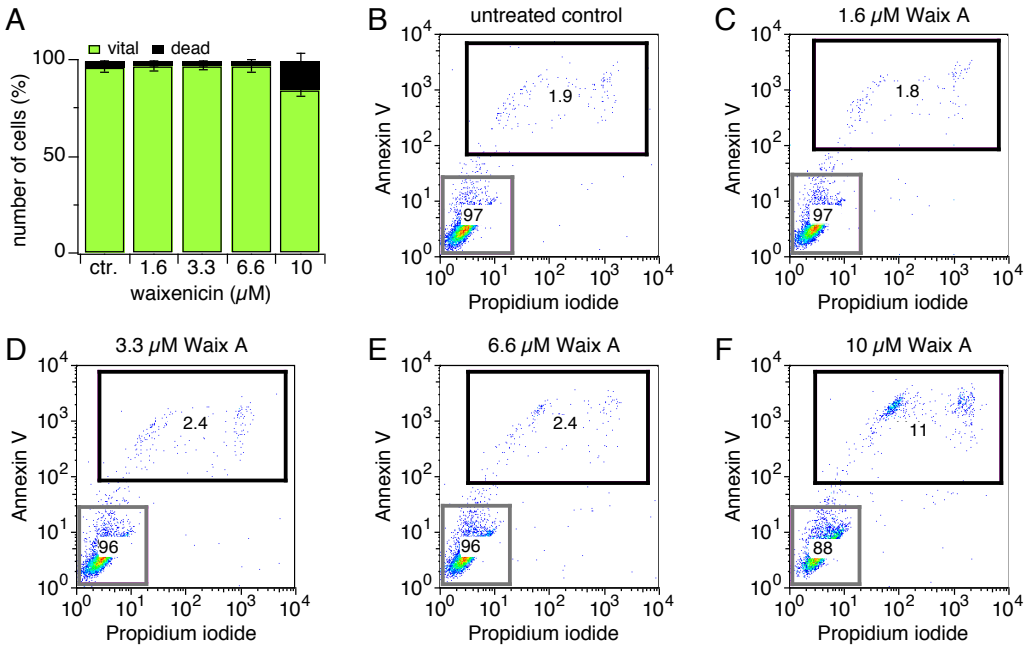

Fig. S5. Toxicity of waixenicin-A is above 10 μM. A. Same data set as in *Fig. 6B*. Averaged, normalized cell count of Annexin-V/PI-stained cells. Data are represented as mean of three independent experiments. Error bars indicate S.E.M. Note an increase in number of dead cells only with the highest compound concentration of 10 μM. *B – F.* Flow cytometric analysis of Annexin-V/PI-stained and waixenicin-A-treated RBL1 cells. Annexin-V-positive cells are plotted against propidium iodide staining. Cells in the lower left quadrant were considered healthy (grey gate), whereas cells in the upper two quadrants (black gate) were considered dead. Untreated control cells *B* versus cells treated with distinct waixenicin-A concentrations: *C*. 1.6 μM, *D*. 3.3 μM, *E*. 6.6 μM and *F*. 10 μM waixenicin-A.

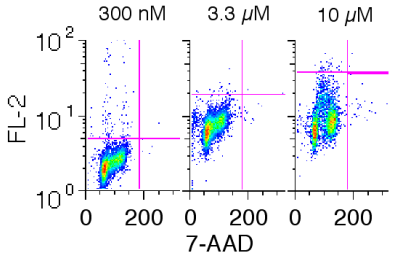

Fig. S6. Waixenicin-A-treated cells exhibit green auto-fluorescence upon excitation with a 488 nM laser. Cell-cycle analysis of Jurkat cells incubated in RPMI medium supplemented with 10% FBS and different waixenicin-A concentrations without BrdU for 2 h. Cells were stained with antiBrdU antibody and 7-AAD and analyzed via flow cytometry. Plots are representative examples for three independent experiments. Note that even without BrdU incorporation, waixenicin-A-treated cells show green fluorescence upon excitation with a 488 nM laser. Emission was collected with a bandpass filter of 530 nm.